Ab initio methods for the optical properties of CdSe clusters

Marie Lopez del Puerto,[1] Murilo L. Tiago,[2,*] and James R. Chelikowsky[1,2,3]
[1]*Department of Physics, University of Minnesota, Minneapolis, Minnesota 55455, USA*
[2]*Center for Computational Materials, Institute for Computational Engineering and Sciences, University of Texas, Austin, Texas 78712, USA*
[3]*Departments of Physics and Chemical Engineering, University of Texas, Austin, Texas 78712, USA*
(Received 8 August 2007; published 2 January 2008)

We have performed time-dependent density functional theory and *GW*/Bethe-Salpeter calculations of the optical properties of a series of CdSe clusters ranging in size from 10 to 82 atoms and passivated by fictitious atoms of half-integer charge. The two methods predict a different character of the optical excitations of the CdSe clusters. In time-dependent density functional theory, the lowest-energy excitation is mainly due to a single-level to single-level transition. In *GW*/Bethe-Salpeter, there is a strong mixture of several different transitions, which is attributed to excitonic effects. Furthermore, *GW*/Bethe-Salpeter calculations predict the presence of dark transitions (optically forbidden) before the first bright transition for all but one of the clusters studied, whereas time-dependent density functional theory predicts the presence of dark transitions for only the two largest clusters. In this paper, we plot and analyze the effective valence and empty state charge densities of these clusters. We determine that the mixing in transitions observed in the *GW*/Bethe-Salpeter calculations is mostly due to the Bethe-Salpeter kernel and not from the fact that quasiparticle wave functions are a linear combination of wave functions obtained from density functional theory. We calculate the radiative decay lifetime of the excitations, and we explain the selection rules that lead to the presence of dark transitions in two of the clusters: $Cd_{17}Se_{28}$ and $Cd_{32}Se_{50}$. Finally, we compare time-dependent density functional theory and *GW*/Bethe-Salpeter absorption spectra to that of Mie theory, which has recently been shown to yield surprisingly accurate results for Si clusters.

DOI: 10.1103/PhysRevB.77.045404 PACS number(s): 71.15.Qe, 73.21.La, 73.61.Ga

I. INTRODUCTION

CdSe clusters are both important and advantageous systems for theoretical study—important because of their remarkable size-dependent optical and electronic properties, with the potential for many technological applications.[1–5] and advantageous because it is possible to synthesize and characterize well-passivated samples with narrow size distributions, as has been shown by several experimental groups[6–10] and which makes comparisons with theory possible.

The challenge, as far as theoretical studies are concerned, is the relative complexity of these systems and of the theories needed to describe them. The ground-state properties of both bare[11] and passivated[12] CdSe clusters have been studied using density functional theory (DFT). Optical and electronic properties, however, are the result of excitations in the system, and thus ground-state theories, such as DFT, are no longer sufficient. This problem has been resolved by extending DFT to time-dependent phenomena.[13–15]

Several clusters have been studied using time-dependent density functional theory (TDDFT), but the results are mixed, sometimes being quite accurate (such is the case of sodium clusters[16]) while at other times giving only a qualitative picture.[17–19] The problem lies in the exchange-correlation potential, since a good general approximation has not been found,[19] resulting in an inaccurate description of systems where excitonic effects are important.

GW/Bethe-Salpeter (*GW*/BSE)[20,21] methods provide an alternate description of time-dependent phenomena, one that does include excitonic effects. There are limited studies of clusters with *GW*/BSE, mostly of small ones with less than 35 atoms,[17,19,22–24] but this method is very accurate for bulk materials,[19,22,23] and the same is expected for finite systems. TDDFT is simpler to implement and is less computationally demanding, while *GW*/BSE is expected to be more accurate, so it is imporant to compare both methods to understand where their differences lie and how one can be improved from insights from the other.

We have previously reported[25] calculations on the excitonic and optical properties of passivated CdSe clusters with up to 82 atoms. In particular, we calculated the energy gap and absorption spectra for a series of clusters (Cd_4Se_6, Cd_8Se_{13}, $Cd_{10}Se_{16}$, $Cd_{17}Se_{28}$, and $Cd_{32}Se_{50}$; their structures are shown in Fig. 1) using the two theoretical approaches mentioned above: TDDFT and *GW*/BSE. We also analyzed the character of the first-allowed transition in these systems.

In this paper, we expand on this previous study. We explain the selection rules that lead to the presence of dark transitions before the first-allowed transition in the time-dependent local density approximation (TDLDA) calculations of $Cd_{17}Se_{28}$ and $Cd_{32}Se_{50}$. We plot and analyze the effective valence and empty state charge densities, calculate the lifetime of excitations, and compare TDLDA and *GW*/BSE absorption spectra to that of Mie theory.

II. METHODOLOGY

A. Real-space pseudopotential method within density functional theory

We calculate ground-state properties, such as the relaxed structure of the clusters, using the real-space pseudopotential

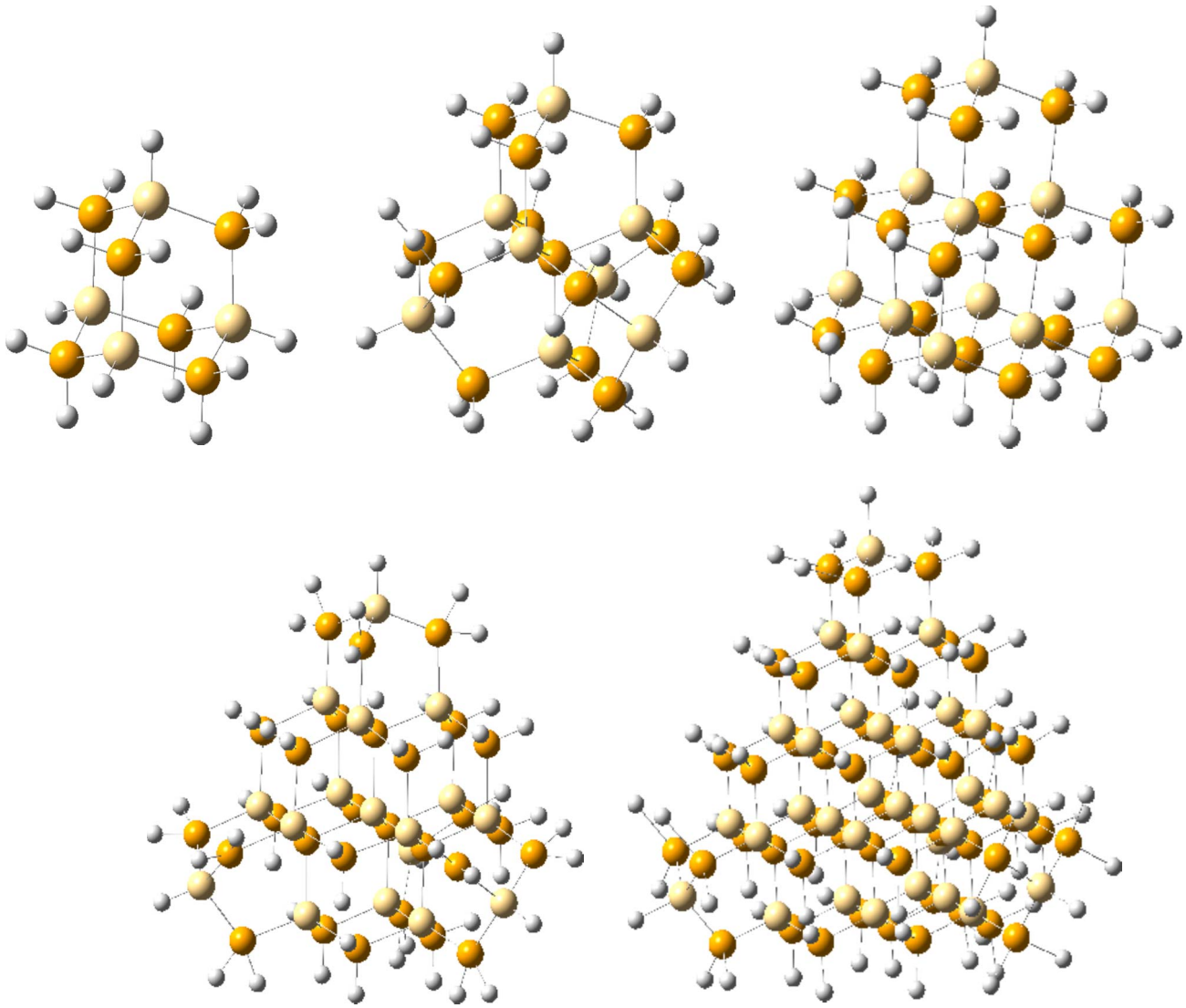

FIG. 1. (Color online) Geometry of the clusters studied: Cd_4Se_6, Cd_8Se_{13}, $Cd_{10}Se_{16}$, $Cd_{17}Se_{28}$, and $Cd_{32}Se_{50}$. Cd atoms are large and dark (yellow online), Se atoms are large and light (light yellow online), and fictitious H atoms are small (gray online).

method within DFT. We describe the electronic problem by a Kohn-Sham equation of the form

$$\left(-\frac{\nabla^2}{2}+\sum_a v_{ion}^p(\mathbf{r}-\mathbf{r}_a)+v_H[\rho(\mathbf{r})]+v_{xc}[\rho(\mathbf{r})]\right)\psi_i(\mathbf{r}) = \epsilon_i\psi_i(\mathbf{r}), \quad (1)$$

where $v_{ion}^p(\mathbf{r}-\mathbf{r}_a)$ is a norm-conserving pseudopotential[26] that replaces the all-electron potential of each ion at $\mathbf{r}_a$, $v_H[\rho(\mathbf{r})]$ is the Hartree potential, and $v_{xc}[\rho(\mathbf{r})]$ is the exchange-correlation potential that is approximated using the LDA. We use atomic units ($\hbar=e=m=1$).

Equation (1) is solved self-consistently on a real-space grid within a spherical boundary (outside of which the wave functions vanish), using a finite-difference expansion for the Laplacian operator. The LDA eigenvalues ϵ_i and eigenfunctions $\psi_i(\mathbf{r})$ are then used as a starting point for the TDDFT and *GW*/BSE calculations. A more detailed description of the real-space pseudopotential method can be found in Refs. 27–30.

The calculations presented in this paper use Cd and Se pseudopotentials that include scalar relativistic effects. There is also a nonlinear core correction in the Cd pseudopotential that accounts for interactions between the 4*d* orbital and the valence orbitals. The initial geometries for the clusters were obtained from the x-ray data[6–8] and were relaxed while conserving tetrahedral symmetry. In order to passivate the clusters, we use fictitious atoms with fractional charges[31] that simulate the effect of organic molecules on the surface of the experimental clusters. Fictitious atoms of charge 1.5*e* (where *e* is the electron's charge) are attached to Cd atoms on the surface, while fictitious atoms of charge 0.5*e* are attached to Se atoms on the surface. The clusters were placed within a spherical boundary with a radius of at least 6 a.u. from the outermost passivating atom. The grid spacing used in the LDA calculations and structure relaxation was 0.3 a.u. A larger grid spacing of 0.6 a.u. was used to calculate optical response as described in the following two subsections.

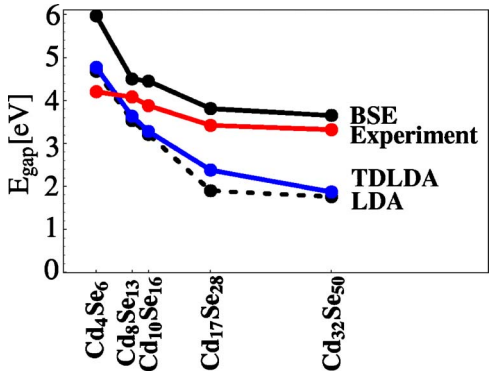

FIG. 2. (Color online) Experimental and calculated (LDA, TDLDA, and *GW*/BSE) optical gaps. The LDA gap is simply the difference between Kohn-Sham eigenvalues. The optical gaps show a strong dependence on cluster size, decreasing with increasing size. The *GW*/BSE calculation follows the experimental trend closely, while the TDLDA calculation deviates from the experimental curve as cluster size increases.

B. Time-dependent density functional theory

In time-dependent density funcitonal theory within the local density approximation, a first-order time-dependent perturbation is introduced to calculate the response of the electronic density to an external potential. This results in an eigenvalue problem of the form[32–34]

$$\mathbf{Q}\mathbf{F}_n = \Omega_n^2 \mathbf{F}_n, \tag{2}$$

with $\mathbf{Q}$ given by

$$Q_{ij\sigma,kl\tau} = \delta_{i,k}\delta_{j,l}\delta_{\sigma,\tau}\hbar^2\omega_{kl\tau}^2 + 2\hbar\sqrt{\lambda_{ij\sigma}\omega_{ij\sigma}}K_{ij\sigma}^{kl\tau}\sqrt{\lambda_{kl\tau}\omega_{kl\tau}}, \tag{3}$$

where $\lambda_{kl\tau}=n_{l\tau}-n_{k\tau}$ is the difference between occupation numbers and $\hbar\omega_{kl\tau}=\epsilon_{k\tau}-\epsilon_{l\tau}$ is the difference between the eigenvalues of the single-particle states. The coupling matrix K describes the linear response of the system. The resulting TDLDA eigenvectors $\mathbf{F}_n$ of Eq. (2) are a linear combination of single-particle transitions from an occupied state to an empty state.

C. GW_f/Bethe-Salpeter

The GW_f/Bethe-Salpeter method is described in detail in Ref. 17, so we present here only a brief outline. The GW_f approximation is the result of an iterative solution of Hedin's equations that includes TDLDA screening, that is, starting from a self-energy of the form $\Sigma(1,2)\sim V_{xc}(1)\delta(1,2)$.[17] This is one step further than the GW_0 approximation where the starting point is $\Sigma(1,2)=0$. In GW_f, the self-energy operator is then the sum of three contributions: One coming from exchange, one from correlation, and one from TDLDA screening. The self-energy corrections are included in the calculation of quasiparticle energies and eigenfunctions by diagonalizing the following eigenvalue equation:[35,36]

$$[H_{LDA} + \Sigma - V_{xc}]\psi_j = E_j\psi_j, \tag{4}$$

where H_{LDA} is the LDA Hamiltonian.

The self-energy from the GW_f approximation and the quasiparticle eigenfunctions obtained from Eq. (4) are the starting point for solving the Bethe-Salpeter equation for the electron-hole correlation function L:

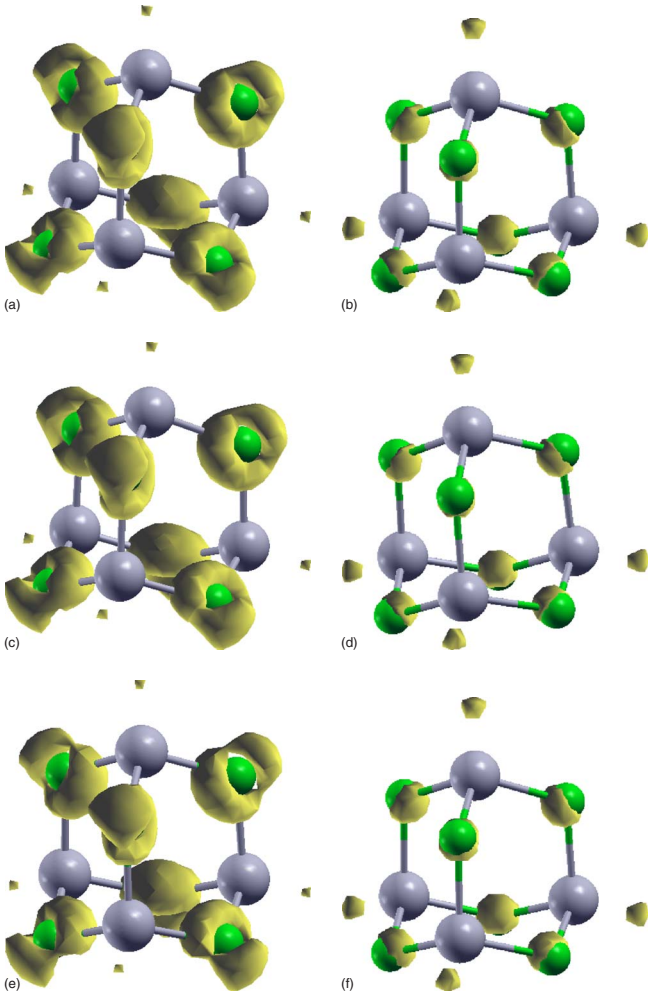

FIG. 3. (Color online) Wave function squared for the HOMO (a) and LUMO (b) of Cd_4Se_6 [Cd atoms are large (gray online), Se atoms are small (green online), passivating atoms are not shown for clarity]. Effective valence charge density (c) and empty state charge density (d) for the TDLDA transition at 4.77 eV. Effective valence charge density (e) and empty state charge density (f) for the *GW*-BSE transition at 5.97 eV. Both TDLDA and *GW*/BSE calculations show little mixing in the transitions of this cluster, which explains the similarity between the three panels.

$$L(1,2;3,4) = G(1,4)G(2,3) + \int d(5678)G(1,5)G(6,3) \times K(5,7;6,8)L(8,2;7,4). \tag{5}$$

K is the kernel operator that describes electron-hole interactions; it is given by

$$K(1,2;3,4) = -i\delta(1,3)\delta(2,4)V(1,2) + \frac{\delta\Sigma(1,3)}{\delta G(4,2)}. \tag{6}$$

As in TDLDA, the BSE excitations are the result of a linear combination of single-particle transitions from an occupied level to an empty level. In both cases, the mixing of transitions is due to the (TDLDA or electron-hole) kernel,

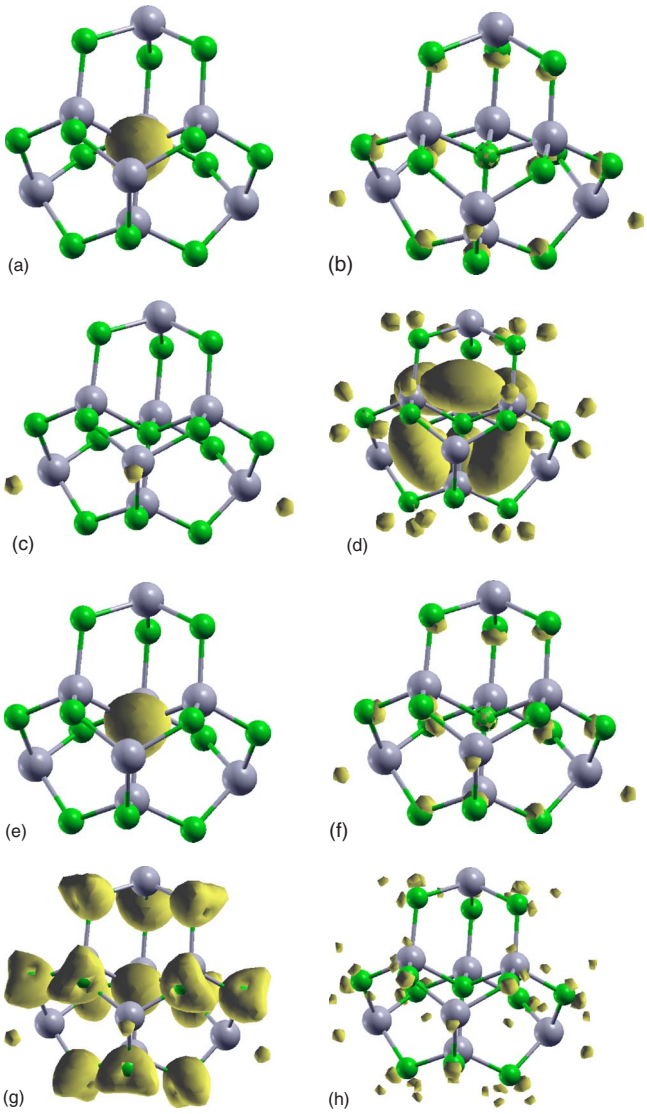

FIG. 4. (Color online) Wave function squared for the HOMO (a) and LUMO (b) of Cd_8Se_{13} [Cd atoms are large (gray online), Se atoms are small (green online)]. Wave function squared for the HOMO-12 (c) and LUMO+5 (d) of Cd_8Se_{13}. Effective valence charge density (e) and empty state charge density (f) for the TDLDA transition at 3.63 eV in Cd_8Se_{13}. This transition is dominated by the HOMO→LUMO transition. Effective valence charge density (g) and empty state charge density (h) for the *GW*-BSE transition at 4.47 eV in Cd_8Se_{13}. This transition is strongly mixed. The largest contribution, HOMO-12→LUMO+5, is responsible for less than 7% of the first peak seen in the *GW*/BSE absorption spectra of this cluster.

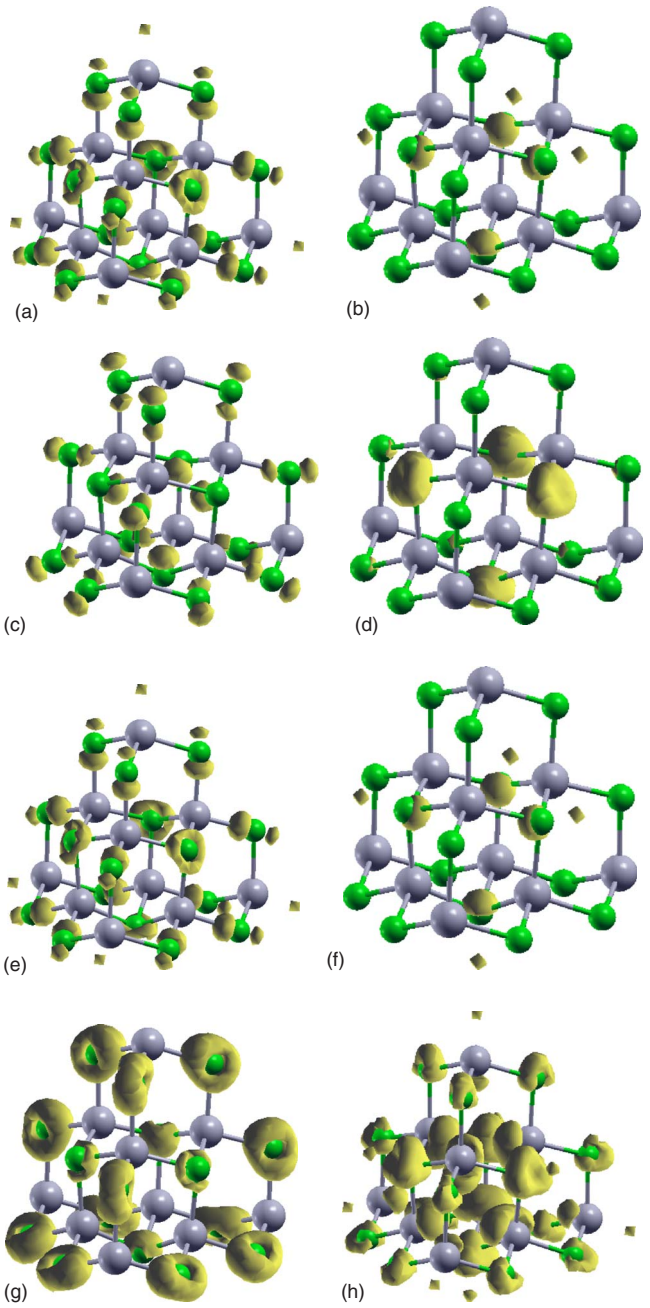

FIG. 5. (Color online) Wave function squared for the HOMO (a) and LUMO (b) of $Cd_{10}Se_{16}$ [Cd atoms are large (gray online), Se atoms are small (green online)]. Wave function squared for the HOMO-11 (c) and LUMO+1 (d) of $Cd_{10}Se_{16}$. Effective valence charge density (e) and empty state charge density (f) for the TDLDA transition at 3.28 eV in $Cd_{10}Se_{16}$. The transition is dominated by the HOMO→LUMO transition. Effective valence charge density (g) and empty state charge density (h) for the *GW*-BSE transition at 4.45 eV in $Cd_{10}Se_{16}$. This transition is strongly mixed; the HOMO-11→LUMO+1 transition contributes ~14%.

but in GW_f/BSE, there is an additional mixing due to the fact that the quasiparticle wave functions are not simply the LDA wave functions but those obtained from Eq. (4).

III. RESULTS

Figure 2 shows the experimental and calculated optical gaps as a function of cluster size, while Fig. 8 shows the absorption cross section calculated with TDLDA and *GW*/BSE. Both the optical gap and the absorption cross section show a strong dependence on cluster size, with the optical gap decreasing quite rapidly with increasing size. The calculations follow the experimental trend for all but the smallest cluster, with LDA and TDLDA gaps ~0.5 to ~1.5 eV below experiment and BSE gaps less than ~0.6 eV above experiment. It is interesting to note that the TDLDA

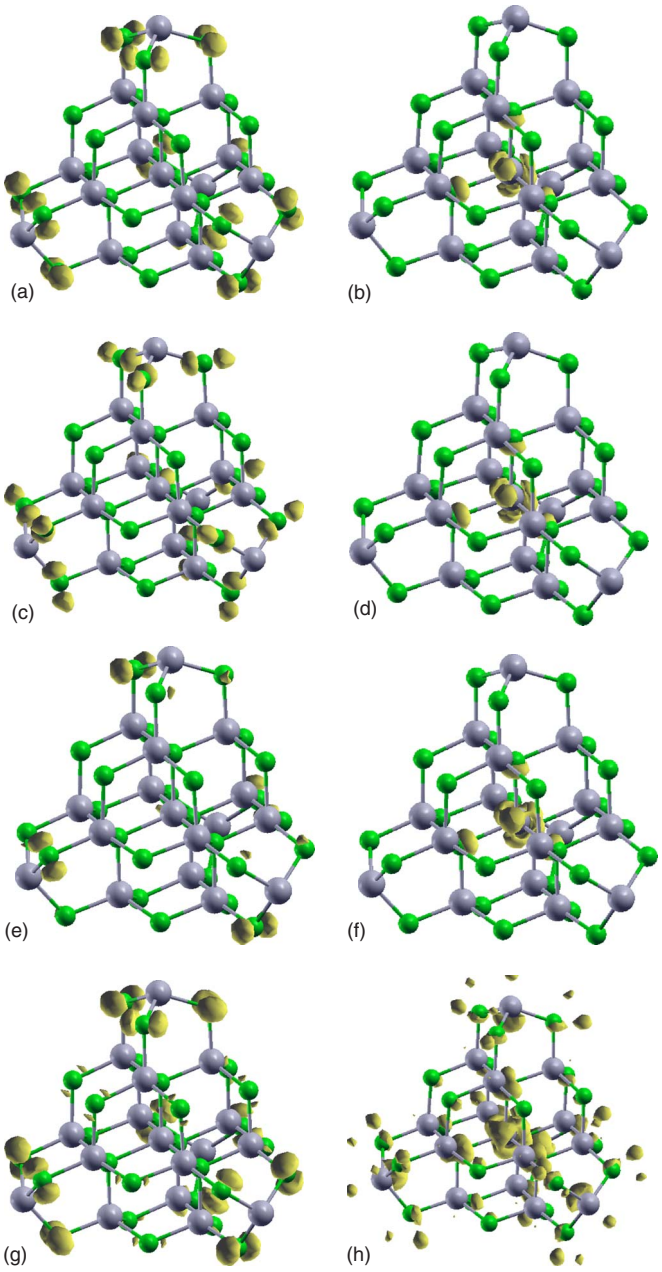

FIG. 6. (Color online) Wave function squared for the HOMO-3 (a) and LUMO (b) of $Cd_{17}Se_{28}$. Wave function squared for the HOMO-24 (c) and LUMO (d) of $Cd_{17}Se_{28}$. Effective valence charge density (e) and empty state charge density (f) for the TDLDA transition at 2.38 eV in $Cd_{17}Se_{28}$. The HOMO-3 → LUMO transition dominates in this case. Effective valence charge density (g) and empty state charge density (h) for the *GW*-BSE transition at 3.87 eV in $Cd_{17}Se_{28}$. This transition is strongly mixed. The HOMO-24 and HOMO-9 levels are the largest contributors.

calculations deviate from the experimental results as cluster size increases, a fact that we explore in the subsections that follow.

A. Effective valence charge and empty state charge density

A useful way of visualizing the mixing of transitions is by plotting the effective valence charge density $\Lambda^n_{valence}$ for a transition at a specific energy Ω_n. $\Lambda^n_{valence}$ is defined as[37]

$$\Lambda^n_{valence}(\mathbf{r}) = \sum_v g^n_v |\phi_v(\mathbf{r})|^2, \tag{7}$$

with $g^n_v = \Sigma_c |F^{vc}_n|^2$. F^{vc}_n are either the TDLDA or BSE eigenvectors and $\phi_v(\mathbf{r})$ are the valence LDA wave functions. When the cluster absorbs energy and undergoes an optical transition, an electron-hole pair is formed. The effective valence charge density gives information about the probability distribution of the hole at each point in space, irrespective of the location of the electron. If there is little mixing, the optical transition will be dominated by a single-level to single-level transition, and the effective valence charge density will basically be proportional to the charge density of the valence level from which the transition originates. In other words, if there is little mixing and the transition at energy Ω_n is dominated by a single-level to single-level transition of the form $a \rightarrow b$ (a transition from an occupied level a to an empty level b), the plot for $\Lambda^n_{valence}$ should closely resemble that of $|\psi_a|^2$. On the other hand, if the mixing is large, $\Lambda^n_{valence}$ will not resemble any given $|\psi_v|^2$, but will have contributions from many of them.

The effective empty state charge density can be defined in a similar way,

$$\Lambda^n_{empty\ state}(\mathbf{r}) = \sum_c g^n_c |\phi_c(\mathbf{r})|^2, \tag{8}$$

summing now over empty state wave functions (as many as were included in the TDLDA or *GW*/BSE calculations). $\Lambda^n_{empty\ state}$ gives information about the probability distribution of the excited electron at each point in space.

The TDLDA calculations of the CdSe clusters show that there is little mixing between transitions (see Table III). For this reason, the plots of effective valence (empty state) charge density for the lowest-energy transition of each cluster closely resembles the plot of the squared valence (empty state) wave function from which the transition originates [Figs. 3(a) and 3(c), 3(b) and 3(d), 4(a) and 4(e), 4(b) and 4(f), 5(a) and 5(e), 5(b) and 5(f), 6(a) and 6(e), 6(b) and 6(f), 7(a) and 7(e), 7(b) and 7(f)). For all effective valence and empty state charge densities, the isosurface plotted is that at half the maximum value.

On the contrary, *GW*/BSE calculations for all but the smallest clusters show that there is strong mixing between transitions. This accounts for the significant difference in Figs. 4(c) and 4(g), 4(d) and 4(h), 5(c) and 5(g), 5(d) and 5(h), 6(c) and 6(g), 6(d) and 6(h), 7(c) and 7(g), 7(d) and 7(h). Mixing in *GW*/BSE comes from two sources: First, in *GW*, the quasiparticle wave functions are a linear combination of LDA wave functions [from the solution of Eq. (4)]; second, in BSE, the electron-hole kernel is stronger and more nonlocal than the TDLDA kernel. In fact, we have previously reported[25] that the mixing in TDLDA is 1 order of magnitude smaller than that in *GW*/BSE.

It is interesting to look at the *GW* and BSE mixings separately. In particular, if the quasiparticle wave functions closely resemble LDA wave functions, then there is little mixing at this level and then the mixing must be attributed to the BSE part of the calculation. We looked at the quasiparti-

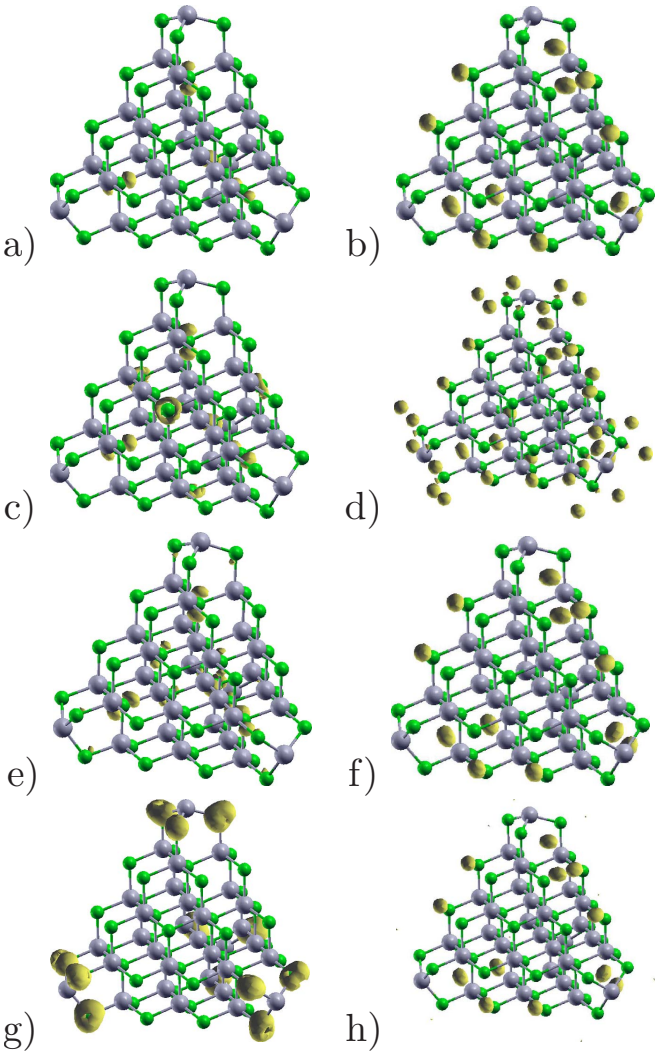

FIG. 7. (Color online) Wave function squared for state HOMO-1 (a) and LUMO (b) of $Cd_{32}Se_{50}$. Wave function squared for state HOMO-13 (c) and LUMO+2 (d) of $Cd_{32}Se_{50}$. Effective valence charge density (e) and empty state charge density (f) for the TDLDA transition at 1.87 eV in $Cd_{32}Se_{50}$. This transition is mostly HOMO-1→LUMO. Effective valence charge density (g) and empty state charge density (h) for the *GW*-BSE transition at 3.65 eV in $Cd_{32}Se_{50}$. This transition is strongly mixed, with the HOMO-13→LUMO+2 transition contributing less than 8%.

cle highest occupied molecular orbital (HOMO) for each cluster, as well as at the levels which we had previously determined to contribute the most to the first energy transition. The projection of quasiparticle wave functions into LDA wave functions is greater than 94% (see Table I). The only exception is the largest cluster, $Cd_{32}Se_{50}$, where two LDA wave functions are mixed with similar weight. The above indicates that there is only a weak mixing that comes from *GW* and the strong mixing comes from BSE since in the end we find that no single valence level contributes more than 25% to the first energy transition.

Comparing the TDLDA and *GW*/BSE effective empty state charge densities, we find that the lowest-energy transition in TDLDA goes to states that are highly localized around the center of the cluster. On the contrary, the

TABLE I. Quasiparticle wave functions as a linear combination of LDA wave functions.

Cluster	Quasiparticle wave function
Cd_4Se_6	$\Psi^{QP}_{HOMO}=0.998\ \Phi^{LDA}_{HOMO}+\cdots$
Cd_8Se_{13}	$\Psi^{QP}_{HOMO}=0.974\ \Phi^{LDA}_{HOMO}+\cdots$
$Cd_{10}Se_{16}$	$\Psi^{QP}_{HOMO}=0.990\ \Phi^{LDA}_{HOMO}+\ldots$
$Cd_{17}Se_{28}$	$\Psi^{QP}_{HOMO}=0.996\ \Phi^{LDA}_{HOMO}+\ldots$
$Cd_{32}Se_{50}$	$\Psi^{QP}_{HOMO}=0.680\ \Phi^{LDA}_{HOMO}+0.722\ \Phi^{LDA}_{HOMO\text{-}1}+\cdots$

GW/BSE lowest-energy transitions tend to go to states that are more delocalized; i.e., the charge is spread around the cluster's outer atoms. This is in agreement with our previous result that the first TDLDA transition goes to the lowest unoccupied molecular orbital (LUMO) or states close to it, while the first *GW*/BSE transition goes to higher (and thus less localized) empty states.

B. Radiative decay lifetimes

Once the TDLDA or *GW*/BSE transition energies and oscillator strengths are known, it is possible to compute radiative decay lifetimes using Fermi's golden rule:

$$dW = 2\pi \sum |\langle i|H_{int}|f\rangle|^2 \delta(E), \tag{9}$$

where $\langle i|$ represents the system in the ground state plus a photon and $|f\rangle$ is the system in the excited state (after absorbing the photon). H_{int} is the interaction Hamiltonian due to the quantized radiation field,[38]

$$H_{int} = e\vec{E}\cdot\vec{r}, \tag{10}$$

$$\vec{E} = \frac{\sqrt{2\pi\hbar w}}{L^{3/2}} \sum_{\vec{k}\lambda} \hat{\epsilon}(a_{\vec{k}\lambda} e^{i\vec{k}\cdot\vec{r}} - a^{\dagger}_{\vec{k}\lambda} e^{-i\vec{k}\cdot\vec{r}}). \tag{11}$$

The transition probability summed over the photon modes and integrated over all angles is then

$$W = \frac{4w^3e^2}{c^3}|\langle\hat{\epsilon}\cdot\vec{r}\rangle|^2, \tag{12}$$

which becomes

$$W = \frac{2w^2e^2f}{c^3} \tag{13}$$

upon substituting the oscillator strength $f=2w|\langle\hat{\epsilon}\cdot\vec{r}\rangle|^2$. The radiative decay lifetime is simply the inverse of Eq. (13).

Table II shows the oscillator strengths and radiative decay lifetimes calculated with both TDLDA and *GW*/BSE for the first-allowed transition of each cluster. The lifetimes are all in the range of tens to hundreds of picoseconds. This is in contrast to the experimentally observed lifetimes, which are much longer, of the order of microseconds.

In the BSE calculations, most clusters show a series of dark transitions (with negligible oscillatory strength) before the first-allowed transition. In the TDLDA calculations, this

TABLE II. Oscillator strengths and radiative decay lifetimes calculated with both TDLDA and *GW*/BSE for the first-allowed transition of each CdSe cluster.

	TDLDA			*GW*/BSE		
Cluster	*E* (eV)	*f*	lifetime (ps)	*E* (eV)	*f*	lifetime (ps)
Cd_4Se_6	4.76	0.19	43.4	5.97	0.63	8.4
Cd_8Se_{13}	3.63	0.27	52.4	4.47	0.40	23.4
$Cd_{10}Se_{16}$	3.28	0.25	69.4	4.45	0.70	13.4
$Cd_{17}Se_{28}$	2.38	0.04	824.0	3.87	0.06	207.8
$Cd_{32}Se_{50}$	1.87	0.45	118.6	3.65	0.98	14.2

only occurs in the two largest clusters (see Table III). Dark transitions, which are a consequence of strong correlations in the BSE kernel, are a signature of excitonic effects. They have been previously observed in small silicon clusters and in bulk semiconductors.[19,22,23] Dark transitions have been shown to attenuate spontaneous emission,[39] which may explain the long radiative lifetimes observed experimentally.

C. Selection rules for $Cd_{17}Se_{28}$ and $Cd_{32}Se_{50}$

The optical properties of clusters can differ considerably from those of the bulk material. In particular, semiconductor clusters do not necessarily have the same direct/indirect gap of bulk due to confinement effects and the fact that the clusters may not retain the bulk geometry.[40,41] Experiments[42] and our own LDA calculations show that bulk CdSe in both

TABLE III. Transitions (denoted as occupied state→empty state) that contribute to the first peak in the absorption spectra of Cd_4Se_6. The Rep. and % columns are the point group representation (B1, B2, and B3 are the representations of a threefold degenerate level) and the percentage of contribution of a particular transition, respectively. The TDLDA transition is dominated by a single-level to single-level transition, while the *GW*/BSE transition is strongly mixed for most clusters.

	TDLDA				*GW*/BSE			
Cluster	Energy (eV)	Rep.	Transition	%	Energy (eV)	Rep.	Transition	%
Cd_4Se_6	4.77	B1, B2, B3	HOMO→LUMO	97.2	5.97	B1, B2, B3	HOMO→LUMO	83.9
			HOMO-2→LUMO+1	1.0			HOMO-1→LUMO+1	8.2
			Other	1.8			Other	7.9
Cd_8Se_{13}	3.63	B1, B2, B3	HOMO→LUMO	97.6	4.47	B1, B2, B3	HOMO-12→LUMO+5	6.0
			HOMO→LUMO+2	0.4			HOMO-7→LUMO+8	4.8
			HOMO-1→LUMO+1	0.3			HOMO-9→LUMO+6	4.6
			Other	1.7			Other	84.6
$Cd_{10}Se_{16}$	3.28	B1, B2, B3	HOMO→LUMO	97.9	4.45	B1, B2, B3	HOMO-11→LUMO+1	14.3
			HOMO-1→LUMO+1	0.6			HOMO-1→LUMO+11	10.6
			Other	1.5			Other	75.1
$Cd_{17}Se_{28}$	2.38	B1, B2, B3	HOMO-3→LUMO	99.4	3.87	B1, B2, B3	HOMO-24→LUMO	12.8
			HOMO-5→LUMO	0.1			HOMO-9→LUMO+3	8.6
			HOMO-2→LUMO+1	0.1			HOMO-8→LUMO+3	5.7
			Other	0.4			Other	72.9
$Cd_{32}Se_{50}$	1.87	B1, B2, B3	HOMO-1→LUMO	98.9	3.65	B1, B2, B3	HOMO-13→LUMO+2	7.6
							HOMO-5→LUMO+9	4.3
			HOMO→LUMO+1	0.4				
							HOMO-12→LUMO+5	4.0
			Other	0.7			Other	83.4

wurtzite and zinc blende configurations is a direct gap semiconductor. Cd_4Se_6, Cd_8Se_{13}, and $Cd_{10}Se_{16}$ also have "direct gaps," i.e., the HOMO-LUMO transition in these clusters is dipole allowed. In all three cases the transition is from a triple-degenerate HOMO to a single-degenerate LUMO.

$Cd_{17}Se_{28}$ has a dipole forbidden HOMO-LUMO transition. This cluster's HOMO and LUMO are both single degenerate and have representation A of point group D_2, such that the direct product $(A \times A)$ is also representation A and thus dipole forbidden. The HOMO-1, HOMO-2, and HOMO-3 are all triple degenerate with representations B_1, B_2, and B_3. The direct product of these states and the LUMO is then $B_x \times A = B_x$, which makes the transitions dipole allowed. However, the oscillator strengths of the HOMO-1 $\rightarrow$LUMO and HOMO-2 $\rightarrow$LUMO transitions are very small, so that the first transition seen in the absorption spectra is actually the HOMO-3 $\rightarrow$LUMO.

As with the three smaller clusters, $Cd_{32}Se_{50}$ has a triple-degenerate HOMO and a single-degenerate LUMO, and a dipole allowed HOMO $\rightarrow$LUMO transition. The oscillator strength for this transition is negligible, though, due to the fact that there is a little overlap between the HOMO and LUMO wave functions (the first closely surrounds surface Se atoms, while the second is distributed in the space between them). The HOMO-1 $\rightarrow$LUMO transition is then the first transition that contributes to the absorption spectra of this cluster.

D. Mie theory

Recent calculations[37] on the absorption spectra of Si clusters comparing TDLDA and Mie theory show a surprisingly good agreement. The expression for the absorption cross section for a (spherical) cluster in vacuum within Mie theory is given by

$$\sigma_{abs}(w) = \frac{9wV}{c} \frac{\epsilon_2(w)}{[\epsilon_1(w)+2]^2 + \epsilon_2(w)^2}, \tag{14}$$

where V is the cluster's volume and $\epsilon_1(w)$ and $\epsilon_2(w)$ are the real and imaginary parts of the dielectric function of the bulk material, which we calculate using the PARATEC (Ref. 43) package.

Figure 8 shows the Mie absorption spectra for the CdSe clusters as compared to the TDLDA and *GW*/BSE calculations. There are two clusters with zinc blende structures, Cd_4Se_6 and $Cd_{10}Se_{16}$. The TDLDA and *GW*/BSE spectra of these clusters are compared to Mie spectra obtained from calculations for bulk CdSe in the zinc blende structure. The other three clusters, Cd_8Se_{13}, $Cd_{17}Se_{28}$, and $Cd_{32}Se_{50}$, have wurtzite structures. The bulk dielectric functions in the parallel and perpendicular directions of wurtzite CdSe were averaged to obtain the Mie wurtzite spectra shown in Fig. 8.

Up to about 8 eV, all three spectra (TDLDA, *GW*/BSE, and Mie) rise gradually, and there is actually a quite good agreement between the three theories, especially for the largest clusters. After 8 eV, the Mie spectra rise more rapidly; the peak is at around 10.5 eV. The TDLDA and *GW*/BSE calculations are not converged beyond 10 eV, so a detailed comparison of peak positions is not possible. However, both the TDLDA and *GW*/BSE spectra seem to peak at higher energies than the Mie spectra.

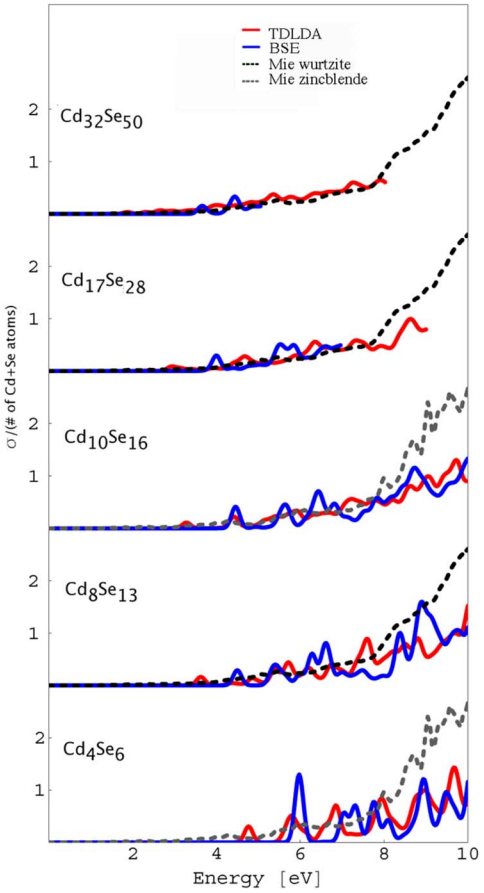

FIG. 8. (Color online) Absorption spectra calculated with Mie theory compared to TDLDA and *GW*/BSE calculations. Two of the clusters have zinc blende structures; Mie theory calculations for these clusters are denoted as "Mie zincblende." The other three clusters are wurtzite structures; Mie theory calculations for the parallel and perpendicular components have been averaged and are denoted as "Mie wurtzite."

IV. CONCLUSIONS

We have analyzed the optical properties of a series of passivated CdSe clusters using two different theoretical methods, one that includes (*GW*/BSE) and one (TDLDA) that does not include excitonic effects. With the latter, we find that the lowest-energy excitation is the result of a single-level to single-level transition and that there are no dark (forbidden) transitions before the first bright transition in most clusters. On the contrary, with the former, we find that it is a strong mixture of different transitions that gives origin to the lowest-energy excitation, a signature that excitonic effects are important. There are also dark transitions before the first bright transition for all but one of the clusters studied.

We have plotted the effective valence and empty state charge density for the lowest-energy excitation as a way of visualizing the mixing between transitions. As there is little mixing in the TDLDA calculations, the effective valence and

empty state charge densities are very similar to the charge density of the LDA valence or empty level from which the transition comes. This is not the case for the plots of the *GW*/BSE effective valence and empty state charge density. Here, the strong mixing means that many LDA valence and empty levels contribute to the transition and thus to the effective charge density.

In order to differentiate between mixing arising from the self-energy correction in *GW* and mixing that comes from solving the Bethe-Salpeter equation, we have looked at the projection of quasiparticle orbitals into LDA orbitals. We find that there is little mixing at the *GW* level, which suggests that it must be the BSE kernel that is responsible for the strong mixing observed.

We have calculated radiative decay lifetimes and find that they are of the order of tens to hundreds of picoseconds. Observed experimental lifetimes are of the order of microseconds, which may be explained by the presence of dark transitions in these clusters. We analyzed the selection rules that lead to dark transitions in the case of $Cd_{17}Se_{28}$ and $Cd_{32}Se_{50}$.

Finally, we compared Mie absorption spectra to that of TDLDA and *GW*/BSE. We find that the initial rise (up to about 8 eV) in the Mie spectra is comparable to the TDLDA and *GW*/BSE calculations. After 8 eV, the Mie spectra rise more rapidly than—and therefore the Mie peak occurs at lower energies than—the maximum of either the TDLDA or *GW*/BSE spectra.

ACKNOWLEDGMENTS

We would like to acknowledge helpful discussions with Xiangyang Huang. This work was supported in part by the National Science Foundation under DMR-0551195 and the U.S. Department of Energy under DE-FG02-06ER15760 and DE-FG02-06ER46286. Calculations were performed at the Minnesota Supercomputing Institute, the Texas Advanced Computing Center, and the National Energy Research Scientific Computing Center (NERSC). M.L.P. would like to acknowledge support from the Louise T. Dosdall Foundation from the University of Minnesota.

*Present address: Materials Science and Technology Division, Oak Ridge National Laboratory, Oak Ridge, TN 37831.

[1] W. Chan and S. Nie, Science **218**, 2016 (1998).
[2] S. Coe, W. Woo, and M. Bawendi, Nature (London) **420**, 800 (2002).
[3] W. Huynh, J. Dittmer, and A. Alivisatos, Science **295**, 2425 (2002).
[4] V. Klimov, A. Mikhailovsky, S. Xu, A. Malko, J. Hollingsworth, C. Leatherdale, H. Eisler, and M. Bawendi, Science **290**, 314 (2000).
[5] X. Michalet, F. Pinaud, L. Bentolila, J. Tsay, S. Doose, J. Li, G. Sundaresan, A. Wu, S. Gambhir, and S. Weiss, Science **307**, 538 (2005).
[6] V. Soloviev, A. Eichhöfer, D. Fenske, and U. Banin, Phys. Status Solidi B **224**, 285 (2001).
[7] V. Soloviev, A. Eichhöfer, D. Fenske, and U. Banin, J. Am. Chem. Soc. **122**, 2673 (2000).
[8] V. Soloviev, A. Eichhöfer, D. Fenske, and U. Banin, J. Am. Chem. Soc. **123**, 2354 (2001).
[9] C. Murray, D. Norris, and M. Bawendi, J. Am. Chem. Soc. **115**, 8706 (1993).
[10] M. Hines and P. Guyot-Sionnest, J. Phys. Chem. **100**, 468 (1996).
[11] M. C. Troparevsky, L. Kronik, and J. R. Chelikowsky, Phys. Rev. B **65**, 033311 (2001).
[12] K. Eichkorn and R. Ahlrichs, Chem. Phys. Lett. **288**, 235 (1998).
[13] E. Runge and E. K. U. Gross, Phys. Rev. Lett. **52**, 997 (1984).
[14] E. K. U. Gross and W. Kohn, Phys. Rev. Lett. **55**, 2850 (1985).
[15] E. Gross and W. Kohn, Adv. Quantum Chem. **21**, 255 (1990).
[16] I. Vasiliev, S. Öğüt, and J. R. Chelikowsky, Phys. Rev. Lett. **82**, 1919 (1999).
[17] M. L. Tiago and J. R. Chelikowsky, Phys. Rev. B **73**, 205334 (2006).
[18] M. Lopez del Puerto, M. L. Tiago, I. Vasiliev, and J. R. Chelikowsky, Phys. Rev. A **72**, 052504 (2005).
[19] G. Onida, L. Reining, and A. Rubio, Rev. Mod. Phys. **74**, 601 (2002).
[20] L. Hedin, Phys. Rev. **139**, A796 (1965).
[21] E. Salpeter and H. Bethe, Phys. Rev. **84**, 1232 (1951).
[22] M. Rohlfing and S. G. Louie, Phys. Rev. B **62**, 4927 (2000).
[23] G. Strinati, Riv. Nuovo Cimento **11**, 1 (1988).
[24] L. X. Benedict, A. Puzder, A. J. Williamson, J. C. Grossman, G. Galli, J. E. Klepeis, J. Y. Raty, and O. Pankratov, Phys. Rev. B **68**, 085310 (2003).
[25] M. Lopez del Puerto, M. L. Tiago, and J. R. Chelikowsky, Phys. Rev. Lett. **97**, 096401 (2006).
[26] N. Troullier and J. L. Martins, Phys. Rev. B **43**, 1993 (1991).
[27] J. R. Chelikowsky, N. Troullier, and Y. Saad, Phys. Rev. Lett. **72**, 1240 (1994).
[28] J. Chelikowsky, J. Phys. D **33**, R33 (2000).
[29] J. Chelikowsky, L. Kronik, and I. Vasiliev, J. Phys.: Condens. Matter **15**, R1517 (2003).
[30] M. M. G. Alemany, M. Jain, L. Kronik, and J. R. Chelikowsky, Phys. Rev. B **69**, 075101 (2004).
[31] X. Huang, E. Lindgren, and J. Chelikowsky, Phys. Rev. B **71**, 165328 (2005).
[32] M. Casida, in *Recent Advances in Density-Functional Methods, Part I*, edited by D. P. Chong (World Scientific, Singapore, 1995).
[33] M. Casida, in *Recent Developments and Applications of Modern Density Functional Theory*, edited by J. M. Seminario (Elsevier Science, Amsterdam, 1996).
[34] I. Vasiliev, S. Öğüt, and J. R. Chelikowsky, Phys. Rev. B **65**, 115416 (2002).
[35] M. S. Hybertsen and S. G. Louie, Phys. Rev. B **34**, 5390 (1986).
[36] W. Aulbur, L. Jönsson, and J. Wilkins, Solid State Phys. **54**, 1 (2000).
[37] J. C. Idrobo, M. Yang, K. A. Jackson, and S. Öğüt, Phys. Rev. B **74**, 153410 (2006).

[38] F. Schwabl, *Advanced Quantum Mechanics* (Springer, New York, 2005).
[39] A. F. van Driel, G. Allan, C. Delerue, P. Lodahl, W. L. Vos, and D. Vanmaekelbergh, Phys. Rev. Lett. **95**, 236804 (2005).
[40] S. H. Tolbert, A. B. Herhold, C. S. Johnson, and A. P. Alivisatos, Phys. Rev. Lett. **73**, 3266 (1994).
[41] M. R. Krishna and R. Friesner, J. Chem. Phys. **95**, 8309 (1991).
[42] A. Edwards and H. Drickamer, Phys. Rev. **122**, 1149 (1961).
[43] J. Iham, A. Zunger, and M. Cohen, J. Phys. C **12**, 4409 (1979); parallel total energy code (PARATEC) (http://www.nersc.gov/projects/paratec/).